Temperature Dependence of Fixed Pattern Noise in Logarithmic CMOS Image Sensors

Dileepan Joseph, *Member, IEEE*, and Steve Collins, *Member, IEEE*

***Abstract*—This paper presents a model that is then simplified to explain the temperature dependence of fixed pattern noise (FPN) in logarithmic complementary metal–oxide semiconductor (CMOS) image sensors. The simplified model uses the average dark response of pixels, which depends only on temperature, to help predict the FPN in the light response, which depends on temperature and illuminance. To calibrate a logarithmic camera, one requires images that are taken at different temperatures and illuminances, which need not be measured, of a uniform stimulus. To correct the FPN in an arbitrary image, one uses the simplified model parameters, which are estimated once by the calibration, and the average dark response, which is infrequently determined by closing the aperture. Through simulation (using mismatch data from a real CMOS process) and experiment (using a commercial logarithmic camera), an improvement is shown in the residual error per image, after calibration, when the proposed method is compared with a related method in the literature that does not account for temperature dependence.**

***Index Terms*—Calibration, complimentary metal–oxide–semiconductor (CMOS) image sensors, fixed pattern noise (FPN), logarithmic response, modeling, temperature dependence.**

I. Introduction

IMAGE sensors are required to operate, like the human eye, over diverse and inconstant temperatures [1]. However, unlike the human eye, image sensors typically do not exist in a homeostatic environment. Due to semiconductor physics, the response of a pixel to illumination may change with temperature. Moreover, a pixel-to-pixel variation of temperature and/or illuminance sensitivity will lead to fixed pattern noise (FPN) in acquired images. For example, the response to a uniform stimulus will not be uniform. Whereas all image sensors must deal with FPN, it is particularly a problem for logarithmic complementary metal–oxide semiconductor (CMOS) image sensors [2]. However, interest in logarithmic cameras persists because they are capable of high-contrast and high-speed imaging [3].

The FPN of logarithmic cameras may be greatly reduced by digital postprocessing of acquired images [4]–[6], which is the focus of this paper. Nonetheless, some researchers prefer analog techniques [7]–[9]. Although several papers, which are summarized below, have been published in recent years that specifically deal with the digital correction of FPN, no prior publication in a peer-reviewed journal has explained the dependence of FPN on temperature. However, an earlier version of this paper, without experimental results or comparison to recent literature, was presented at a conference [10]. Moreover, this paper is derived, with much revision, from a Ph.D. thesis [11].

Previously, Joseph and Collins [12] have explained FPN in logarithmic cameras at one temperature. They modeled, calibrated, and corrected pixel responses to the limit of quantization noise. Shortly thereafter, they extended the work to color rendition [13], demonstrating a postrendition image quality that is comparable to conventional linear cameras. More recently, they have explained how FPN may be caused by the transient response of the read-out circuit [14], in addition to the steady-state response of the system. Meanwhile, Choubey *et al.* [15] have experimented with electronic self-calibration, and Otim *et al.* [16] have simplified the calibration and correction algorithms. Independent researchers in the academy and the industry have seen value in some of these works [4]–[6].

Further in the past, Marshall and Collins [17] and Loose *et al.* [8] have noted that temperature would affect the threshold voltage variation in logarithmic CMOS image sensors. They wrote that uniform temperature dependence would be less problematic than nonuniformity in the temperature dependence of pixel responses; however, the dependence was never characterized. Instead, Marshall and Collins suggested a digital method to correct FPN that considered both temperature and illumination dependence. They advocated using an autofocus system to defocus a scene to obtain a calibration image that may then be subtracted from the focused image of the scene. This approach required frequent mechanical operation and introduced spatial high-pass filtering to the image, proving unsuitable when rendering images for human observers.

While this paper was undergoing peer review, Schneider [4] and Hoefflinger [6] published a Ph.D. excerpt and a book chapter, respectively, that address the temperature dependence of FPN in logarithmic CMOS image sensors. As with this paper, their work extends the established model of Joseph and Collins, but their approach differs from the one taken here. Their work is based on empirical observation, whereas this paper is based on semiconductor physics. Moreover, the method of Schneider and Hoefflinger requires the measurement of temperature and illuminance for calibration and the measurement of temperature for correction, whereas the method proposed here requires no such measurement. Furthermore, the statistical basis of their calibration is unclear, whereas the calibration discussed here is based on the maximum-likelihood estimation.

Section II models the response of a logarithmic pixel to temperature and illuminance. Section III describes the calibration

Manuscript received September 4, 2007; revised October 31, 2008. First published April 24, 2009; current version published July 17, 2009. This work was supported by the Natural Sciences and Engineering Research Council of Canada and the Engineering and Physical Sciences Research Council of the U.K.

D. Joseph is with the Department of Electrical and Computer Engineering, University of Alberta, Edmonton, AB T6G 2V4, Canada (e-mail: dil.joseph@ualberta.ca).

S. Collins is with the Department of Engineering Science, University of Oxford, OX1 3PJ Oxford, U.K. (e-mail: collins@robots.ox.ac.uk).

Digital Object Identifier 10.1109/TIM.2009.2014618

of a sensor using images of a uniform scene that are taken at different temperatures and with different illuminances. As calibration may be a costly process, emphasis is placed on eliminating temperature and illuminance measurement, and on simplifying the model so that only arithmetic operations are required. Finally, Sections IV and V evaluate the simplified model and its calibration via simulation and experiment, respectively.

II. Modeling

In a typical logarithmic CMOS image sensor, the digital response y of a pixel depends on the light stimulus x falling on the pixel according to the model [12]

$$y = a + b\ln(c + x) + \epsilon \tag{1}$$

with an offset

$$a = F_{\mathrm{ADC}} + G_{\mathrm{ADC}} \times \left(V_{DD} - V_{on}^{\mathrm{T1}} - V_T^{\mathrm{T2}} - V_T^{\mathrm{T5}} - \sqrt{\frac{K^{\mathrm{T4}}}{K^{\mathrm{T2}}}}\left(V_{GS}^{\mathrm{T4}} - V_T^{\mathrm{T4}}\right) - \sqrt{\frac{K^{\mathrm{T7}}}{K^{\mathrm{T5}}}}\left(V_{GS}^{\mathrm{T7}} - V_T^{\mathrm{T7}}\right) + \frac{n^{\mathrm{T1}}kT}{q}\ln\frac{I_{on}^{\mathrm{T1}}}{G_A G_L G_Q A} \right) \tag{2}$$

a gain

$$b = -G_{\mathrm{ADC}}\frac{n^{\mathrm{T1}}kT}{q} \tag{3}$$

and a bias

$$c = \frac{I_S}{G_A G_L G_Q A}. \tag{4}$$

The error ϵ, which is made up of quantization, temporal, and approximation noise, is assumed to be independent of temperature T and illuminance x. Superscripts above identify the ownership of parameters by the numbered transistors in [12, Fig. 1], which is the source of (1)–(4). For example, V_{GS}^{T4} and V_{GS}^{T7} determine the bias currents for the column and output source followers, respectively. Furthermore, F_{ADC} and G_{ADC} are the offset and the gain of the analog-to-digital converter (ADC), V_{DD} is the supply voltage, and G_A, G_L, and G_Q are the gains due to the aperture, the lens, and the quantum efficiency, respectively. Other circuit parameters are described below.

The offset a in (2), which is an abstract parameter that incorporates a number of physical parameters, is affected by temperature in several ways. To begin with, threshold voltages V_T have linear dependence on temperature, and current gains K depend on temperature by a power law, i.e.,

$$V_T = V_{T0} - TCV(T - T_{\mathrm{ref}}) \tag{5}$$

$$K = K_0\left(\frac{T}{T_{\mathrm{ref}}}\right)^{BEX}. \tag{6}$$

These equations come from the HSPICE Level 28 model [18], as simpler models do not consider the temperature dependence of V_T or K. T_{ref} is a reference temperature, which is measured in degrees Kelvin as with T. V_{T0} and K_0 are the threshold voltage and the current gain at that temperature, respectively. The multiplier TCV and the exponent BEX define how quickly the threshold voltage and the current gain change with temperature. For simplicity, this paper assumes that BEX is constant across devices.

The parameter V_{on} in (2), which is taken from the Level 3 model [18], signifies the gate–source voltage at which a transistor changes from the weak to the strong inversion region of operation. This threshold linearly depends on temperature, i.e.,

$$V_{on} = V_T + \frac{nkT}{q}. \tag{7}$$

The parameter I_{on} in (2) is the drain–source current at the gate–source voltage V_{on}. Its dependence on temperature may be found using the Level 1 model [18] of the current in the saturation region (ignoring the finite output resistance), i.e.,

$$I_{on} = K\left(\frac{nkT}{q}\right)^2. \tag{8}$$

Assuming an ideal ADC, gain b depends on temperature in only one way, as shown in (3). The relationship comes from the Level 3 model [18], wherein the slope of the subthreshold response (V_{DS} versus the logarithm of I_{DS}) of a diode-connected transistor (where V_{GS} is equal to V_{DS}) is a multiple of temperature, i.e.,

$$V_{DS} = \frac{nkT}{q}\ln\frac{I_{DS}}{I_{on}} + V_{on}. \tag{9}$$

In this equation, n is an ideality factor, k is the Boltzmann constant, and q is the electron charge.

Neglecting any dependence of the aperture, lens, and quantum efficiency gains on temperature, the bias c in (4) depends on temperature in only one way also. In the simplest case [18], the reverse bias saturation current of the photodiode is an exponential function of temperature, i.e.,

$$I_S = I_{S0}e^{T/T_e}. \tag{10}$$

The parameter T_e is equal to about $(7/\ln 2)$ K since I_S doubles approximately every 7 K [1]. Although I_{S0} may vary from device to device, the variation of T_e is neglected for simplicity.

Factoring the above temperature dependencies of physical parameters out of (2)–(4), response y of a logarithmic pixel to temperature T and illuminance x is given by (1) with a temperature-dependent offset

$$a(T) = a_1 + a_2T + a_3T\ln T \tag{11}$$

a temperature-dependent gain

$$b(T) = b_1T \tag{12}$$

and a temperature-dependent bias

$$c(T) = c_1e^{T/T_e}. \tag{13}$$

Proto-offsets a_1, a_2, and a_3, protogain b_1, and protobias c_1 may be written in terms of circuit parameters if required [11]; however, this is not necessary for FPN calibration or correction.

As noted by Marshall and Collins [17], there is no temperature-dependent FPN if pixel responses uniformly

depend on temperature. However, based on the above model, a pixel-to-pixel variation of a_2, a_3, b_1, c_1, or any combination thereof would cause temperature-dependent FPN in a logarithmic camera (N.B. a_1 is not in any way connected to T). Since it is known that offsets, gains, and biases all vary in a logarithmic camera [12], FPN *must* depend on temperature.

Through empirical observation, Schneider [4] and Hoefflinger [6] proposed instead the following extension to (1), with T in degrees Celsius:

$$a(T) = a_0 + \alpha T \tag{14}$$

$$b(T) = b_0 + \beta T \tag{15}$$

$$c(T) = c_0 + \gamma T. \tag{16}$$

Since T in (11) is in degrees Kelvin, and normal operating temperatures for a camera are around 300 K, a linear approximation of $T \ln T$ proves accurate and is used in this paper. Hence, the theoretical prediction in (11) agrees with the empirical observation in (14).

Given that T in (15) is in degrees Celsius, (12) and (15) are equivalent for $b_0 = (273\ \text{K})b_1$ and $\beta = b_1$. However, Hoefflinger's data show that $b_0 = (-102\ \text{K})\beta$ and not $b_0 = (273\ \text{K})\beta$; therefore, there is still a discrepancy. Nonetheless, Hoefflinger affirms (9), which implies (12), without noting the contradiction with (15). Recently, it has been shown that the transient response of the read-out circuit may inadvertently determine the gain in a logarithmic camera [14], which may explain this discrepancy. With due attention to the read-out circuit (and the ADC), however, (12) should apply.

Another discrepancy exists, this time between (13) and (16). Hoefflinger's data purport to show that dark current linearly depends on temperature; however, this contradicts the well-known exponential dependence. Careful reading of Schneider's Ph.D. work, on which Hoefflinger's data are based, suggests that this discrepancy is due to a typographical error. The data may refer to $c' = \ln c$ and not to c itself. An empirical observation that c' linearly depends on T (in degrees Celsius), i.e., $c' = c'_0 + \gamma T$, would agree with (13) for $c'_0 = \ln c_1 + (273\ \text{K})/T_e$ and $\gamma = 1/T_e$. With this interpretation, one calculates $T_e = (12.6/\ln 2)$ K from Hoefflinger's data, which is 80% greater than the value reported by El Gamal and Eltoukhy [1]. However, the empirical observations of Schneider and Hoefflinger are vulnerable to statistical bias, as explained in Section III.

III. Calibration

In the study of linear charge-coupled-device and CMOS image sensors, it is well known that the response of pixels with the aperture of the camera closed, which is called the *dark response*, is a function of temperature. In reality, this dark response also bears upon the response of the pixels with the aperture open (i.e., to a focused image), which is called the *light response*. As the dark response is only affected by temperature and not illuminance, it may be used to calibrate and correct temperature-dependent FPN in the light response. Illumination-dependent FPN, which is also present, may be corrected using a method that is similar to the one established in the literature.

To correct the FPN in an image sensor, one estimates the parameters that vary from pixel to pixel and compensates accordingly. For the model in (1), three types of illumination-dependent FPN have been examined in the literature [12]: 1) single variation, where only a varies; 2) double variation, where a and b vary; and 3) triple variation, where a, b, and c vary. Given the images of a uniform scene, which are taken at different illuminances but at one temperature, the single- and double-variation models were calibrated by linear regression, permitting an analytic solution, and the triple-variation model was calibrated by nonlinear optimization, requiring an iterative solution.

To calibrate a sensor having N pixels over both temperature and illuminance, images are taken from a uniform scene at L different temperatures T_h, where $1 \le h \le L$, and M different nonzero illuminances x_i, where $1 \le i \le M$. These $L \times M$ images comprise the *light* response of the sensor. Images are also taken at the same temperatures but with zero illuminance, e.g., by closing the aperture of the camera. These L images comprise the *dark* response of the sensor. At the hth temperature and the ith illuminance, the *actual* light and dark responses of the jth pixel, where $1 \le j \le N$, are denoted by y_{hij} and y_{h0j}, respectively. Using (1) and (11)–(13), these responses are *predicted* by

$$\tilde{y}_{hij} = a_{1j} + a_{2j}T_h + a_{3j}T_h \ln T_h + b_{1j}T_h l_{hi} \tag{17}$$

$$\tilde{y}_{h0j} = a_{1j} + a_{2j}T_h + a_{3j}T_h \ln T_h + b_{1j}T_h l_{h0} \tag{18}$$

where

$$l_{hi} = \ln(c_1 e^{T_h/T_e} + x_i) \tag{19}$$

$$l_{h0} = \ln(c_1 e^{T_h/T_e}). \tag{20}$$

The differences between the actual responses y_{hij} and y_{h0j} and the predicted responses $\tilde{y}_{hij}$ and $\tilde{y}_{h0j}$ are the error terms ϵ_{hij} and ϵ_{h0j}, which are assumed to be independent from sample to sample and to follow a zero-mean Gaussian distribution.

Note that (17) and (18) allow a variation of the proto-offsets a_1, a_2, and a_3, as well as the protogain b_1, from pixel to pixel, which totals $4N$ variables. However, (19) and (20) assume that the protobias c_1, as well as the exponential factor T_e, is constant for all pixels, which adds another two variables only. Although bias variation does exist in logarithmic cameras [12], it has been ignored here to avoid nonlinear optimization.

Whereas temperatures T_h and illuminances x_i may be measured, albeit with some uncertainty, calibration would be simpler and more robust if their values were not required. Fortunately, there is a way to calibrate the image sensor while avoiding the measurement of T_h and x_i. This method relies on two observations, namely, that the averages taken over all pixels of the actual and predicted responses are interchangeable for either the light or the dark case, i.e.,

$$\frac{1}{N}\sum_{j=1}^{N} y_{hij} \approx \frac{1}{N}\sum_{j=1}^{N} \tilde{y}_{hij} \tag{21}$$

$$\frac{1}{N}\sum_{j=1}^{N} y_{h0j} \approx \frac{1}{N}\sum_{j=1}^{N} \tilde{y}_{h0j}. \tag{22}$$

These approximations are good when there are many pixels because averaging reduces the variance of the error terms, i.e., the difference between actual and predicted responses.

Denoting the left sides of (21) and (22) by $\bar{y}_{hi}$ and $\bar{y}_{h0}$, which are called the average light and dark responses, respectively, and substituting (17) and (18) into the right sides give

$$\bar{y}_{hi} \approx \bar{a}_1 + \bar{a}_2 T_h + \bar{a}_3 T_h \ln T_h + \bar{b}_1 T_h l_{hi} \tag{23}$$
$$\bar{y}_{h0} \approx \bar{a}_1 + \bar{a}_2 T_h + \bar{a}_3 T_h \ln T_h + \bar{b}_1 T_h l_{h0} \tag{24}$$

where $\bar{a}_1$, $\bar{a}_2$, and $\bar{a}_3$ are the average proto-offsets, which are taken over all pixels, and $\bar{b}_1$ is the average protogain. Examination of (20) and (24) shows that $\bar{y}_{h0}$ is a function of T_h with temperature-independent constants $\bar{a}_1$, $\bar{a}_2$, $\bar{a}_3$, $\bar{b}_1$, $\bar{c}_1$, and T_e. Thus, temperature need not be measured since the average dark response may be used in proxy.

To eliminate the measurement of x_i, which appears in (17) and (23) due to (19), one substitutes the left side of (23) into the right side of (17) to give

$$\tilde{y}_{hij} \approx a'_{1j} + a'_{2j} T_h + a'_{3j} T_h \ln T_h + b'_{1j} \bar{y}_{hi} \tag{25}$$

with a normalized protogain

$$b'_{1j} = b_{1j} / \bar{b}_1 \tag{26}$$

and normalized proto-offsets

$$a'_{kj} = a_{kj} - b'_{1j} \bar{a}_k \tag{27}$$

where $1 \le k \le 3$.

What remains is to eliminate T_h in (25) using $\bar{y}_{h0}$ in (24). The nonlinearities $T_h \ln T_h$ and $T_h l_{h0}$, where l_{h0} is a function of T_h by (20), make this seem impossible. However, assuming $\bar{y}_{h0}$ approximates a linear function of T_h over the temperature range of interest, $T_h \ln T_h$ and $T_h l_{h0}$ may be linearized. Using Taylor expansion around an operating point $\bar{T}$, one finds

$$T_h \ln T_h \approx T_h (1 + \ln \bar{T}) - \bar{T} \tag{28}$$
$$T_h l_{h0} \approx T_h (\ln c_1 + 2\bar{T}/T_e) - \bar{T}^2 / T_e. \tag{29}$$

Consequently, the left side of (24) may be substituted into the right side of (25) to give

$$\tilde{y}_{hij} \approx a''_{1j} + a''_{2j} \bar{y}_{h0} + b'_{1j} \bar{y}_{hi} \tag{30}$$

with linearized proto-offsets

$$a''_{lj} = \frac{1}{d_{11}} \sum_{k=1}^{3} d_{lk} a'_{kj} \tag{31}$$

where $1 \le l \le 2$, and where d_{lk} are the linearization coefficients that are independent of temperature or illuminance. Using (25)–(31), exact formulas for d_{lk} may be derived [11].

Equation (30), which is called the *temperature proxy* model, shows that the predicted light response of any pixel is approximately a linear function of the average dark and light responses of all pixels, given the same temperature and illuminance. There is no need to determine any of the linearization coefficients d_{lk} in (31) if linearized proto-offsets a''_{lj} and normalized protogain b'_{1j} in (30) are estimated directly. These unknowns are estimated for all pixels by minimizing the sum of squared error (SSE) between the actual and predicted light responses, i.e.,

$$\text{SSE}\left(a''_{1j}, a''_{2j}, b'_{1j}\right) = \sum_{h=1}^{L} \sum_{i=1}^{M} \sum_{j=1}^{N} (y_{hij} - \tilde{y}_{hij})^2. \tag{32}$$

Using multilinear algebra [11], the estimated parameters are

$$\hat{\mathbf{b}}_j = \left(\sum_{h=1}^{L} \sum_{i=1}^{M} \bar{\mathbf{y}}_{hi}^{\mathrm{T}} \bar{\mathbf{y}}_{hi}^{-1} \right) \left(\sum_{h=1}^{L} \sum_{i=1}^{M} \bar{\mathbf{y}}_{hi}^{\mathrm{T}} y_{hij} \right) \tag{33}$$

where

$$\hat{\mathbf{b}}_j = \begin{pmatrix} \hat{a}''_{1j} & \hat{a}''_{2j} & \hat{b}'_{1j} \end{pmatrix}^{\mathrm{T}} \tag{34}$$
$$\bar{\mathbf{y}}_{hi} = \begin{pmatrix} 1 & \bar{\mathbf{y}}_{h0} & \bar{y}_{hi} \end{pmatrix}. \tag{35}$$

Note that, in addition to the $3N$ variables $\hat{a}''_{1j}$, $\hat{a}''_{2j}$, and $\hat{b}'_{1j}$, which are calculated from the actual light response y_{hij} according to (33), the LM variables $\bar{y}_{hi}$ are also calculated from the same response according to the left side of (21). Thus, there are

$$P = LM + 3N \tag{36}$$

model parameters that are *explicitly* fitted to the acquired data. Using only (33)–(35) and the definition of $\bar{y}_{hi}$, one can prove that

$$\frac{1}{N} \sum_{j=1}^{N} \begin{pmatrix} \hat{a}''_{1j} & \hat{a}''_{2j} & \hat{b}'_{1j} \end{pmatrix} = \begin{pmatrix} 0 & 0 & 1 \end{pmatrix} \tag{37}$$

which means that three parameters may be calculated without using the data. Thus, there are actually

$$Q = LM + 3N - 3 \tag{38}$$

parameters that are *implicitly* fitted to the data. An alternative interpretation is that three extra conditions result from the process by which measurements have been eliminated.

The term inside the parentheses on the right-hand side of (32) is merely the error term ϵ_{hij}. Thus, an estimate of the error variance may be found by dividing the minimized SSE by the corresponding degrees of freedom, i.e.,

$$\hat{\sigma}_\epsilon^2 = \frac{\text{SSE}\left(\hat{a}''_{1j}, \hat{a}''_{2j}, \hat{b}'_{1j}\right)}{LMN - Q}. \tag{39}$$

The denominator is equal to the number of responses LMN minus the number of implicit parameters Q that are fitted to those responses (using P would be slightly incorrect) [11].

In theory, the estimated variance of the error term has the same expected value even if the estimate was made using data from one temperature and illuminance only, i.e., using one image only. Thus, the SSE per image, which is a function of temperature and illuminance, is given by

$$\text{SSE}_{hi}\left(a''_{1j}, a''_{2j}, b'_{1j}\right) = \sum_{j=1}^{N} (y_{hij} - \tilde{y}_{hij})^2 \tag{40}$$

and the estimate of the error variance per image is given by

$$\hat{\sigma}^2_{\epsilon_{hi}} = \frac{\mathrm{SSE}_{hi}\left(\hat{a}''_{1j}, \hat{a}''_{2j}, \hat{b}'_{1j}\right)}{N - Q/LM}. \tag{41}$$

For brevity, the square roots of the estimated variances in (39) and (41), which represent the estimated standard deviations, are called the *residual error* and the *residual error per image*, respectively. These statistics are useful in assessing the temperature proxy method of calibration.

The above calibration was derived for images taken at all combinations of L temperatures T_h and M illuminances x_i. In practice, the temperature of the image sensor is varied, and, at each set point, the illuminance of the uniform scene is varied. However, it may be difficult to ensure that the illuminance set points are the same from one temperature set point to another. In the worst case, LM different illuminances, which are denoted by x_{hi}, would occur. Fortunately, this change does not affect any of the above results. Although l_{hi} in (19) must be rewritten as

$$l_{hi} = \ln(c_1 e^{T_h/T_e} + x_{hi}) \tag{42}$$

none of the other equations need to be altered.

Only a few formulas presented above require implementation. The left sides of (21) and (22) give $\bar{y}_{hi}$ and $\bar{y}_{h0}$, whereas (33) gives $\hat{a}''_{1j}$, $\hat{a}''_{2j}$, and $\hat{b}'_{1j}$. Other formulas were presented to explain the method and provide a means for assessment. Although (33) incorporates matrix inversion and matrix-vector multiplication, it may be implemented more efficiently using Gaussian elimination. In any case, the calibration requires only arithmetic operations.

The calibration needs to be done only once. To correct the FPN in an arbitrary image y_{1j} at any temperature, one requires a dark image y_{0j} at the same temperature, which may be infrequently taken with a closed aperture—the temperature of the image sensor is unlikely to change quickly. A similar analysis to the above shows that the corrected image y_{2j} is given by

$$y_{2j} = \left(y_{1j} - \hat{a}''_{1j} - \hat{a}''_{2j}\bar{y}_0\right)/\hat{b}''_{1j} \tag{43}$$

where $\bar{y}_0$ is the mean of the dark image. Thus, the correction also requires only arithmetic operations, which makes it suitable for real-time implementation.

As noted at the beginning of this section, bias variation has been neglected. To consider it, one must replace l_{hi} and l_{h0} in (17) and (18) with l_{hij} and l_{h0j}, respectively, where

$$l_{hij} = \ln(c_{1j} e^{T_h/T_e} + x_{hi}) \tag{44}$$

$$l_{h0j} = \ln(c_{1j} e^{T_h/T_e}). \tag{45}$$

With these changes, it is still possible to derive a calibration that eliminates the measurement of T_h and x_{hi}. However, whether either of these measurements are eliminated, nonlinear optimization seems unavoidable. Further work is needed to find a well-defined heuristic to approximate the nonlinear optimization in a fixed number of arithmetic operations. In the meantime, the literature shows that correction of only offset and gain variation sufficiently reduces the FPN for all scenes, or parts thereof, that are not illuminated dimly [6], [12].

In their method of calibration, Schneider [4] and Hoefflinger [6] also use $L \times M$ images of a uniform scene, which are taken at L temperatures and M illuminances with N pixels per image, as expressed with the symbols of this paper. First, for each pixel, they perform L independent calibrations with respect to illuminance to estimate a, b, and c at each temperature. These calibrations are not regressions. Instead of using all M points at once to obtain the estimates, several subsets are used independently, and the results are then combined. It is like taking two points at a time, in the context of finding a "best fit" line for a set of points, to estimate the intercept and the slope, and then averaging over many such estimates. Second, for each pixel, Schneider and Hoefflinger perform three independent regressions—on the estimated offsets, gains, and biases (or log biases)—with respect to temperature to estimate a_0, α, b_0, β, c_0 (or c'_0), and γ, which are the temperature-independent parameters from (14)–(16). This makes a total of LN independent calibrations on the measured data followed by $3N$ independent regressions on the calibration estimates.

The statistical basis of Schneider and Hoefflinger's method is not clear. In contrast, the temperature proxy method is based on the maximum-likelihood estimation [11], which makes it robust to measurement error, e.g., due to quantization and temporal noise. First, a generative model is used to explain how the independent variables, model parameters, and additive Gaussian noise generate the measured data. Second, a single regression is performed over the measured data to estimate in one step the parameters of the generative model after simplification in a logical fashion. The least squares method thereby equates to the maximum-likelihood estimation.

Finally, Schneider and Hoefflinger's method requires the measurement of temperature and illuminance to perform calibration and the measurement of temperature to perform correction. The temperature proxy method requires no such measurement.

IV. Simulation

A logarithmic CMOS image sensor, with circuits as drawn in [12, Fig. 1], was simulated using Cadence for a 0.35-μm 3.3-V process from Austria Microsystems (AMS). Avoiding optical considerations, stimulus x was represented by an ideal current source, in parallel with the reverse-biased diode in the pixel. The ADC was not simulated, and, therefore, what would be the ADC input voltage was taken as the response y. These changes affect neither the abstract model of Section II nor the calibration method of Section III.

Transistors and diodes were simulated using the BSIM3 Version 3 models [18], with parameters supplied by AMS [19]. Considering the process design rules [20], the nominal width and length of all transistors were set to 1 and 0.6 μm, respectively. A model that describes the p-n junction between the n-type diffusion and the p-type substrate was used to represent diodes. As these diodes simulated photodiodes in pixels, they were set to a 6.32×6.32 μm size, which corresponds to a photosensitive square in a 10×10 μm pixel with a 40% fill factor—the specifications of the HDRC VGA 2 logarithmic

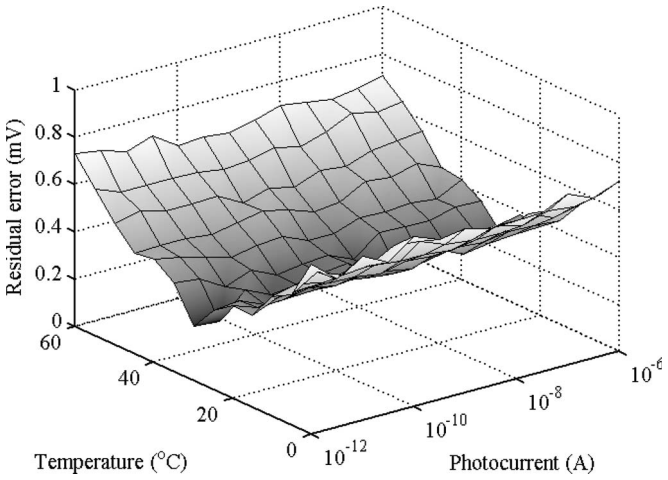

Fig. 1. Residual error per image versus temperature and photocurrent for the calibration of the established double-variation model [12] to simulated data at 30 °C with subsequent extrapolation to other temperatures. The overall residual error is 0.49 mV or 1.2% of a decade.

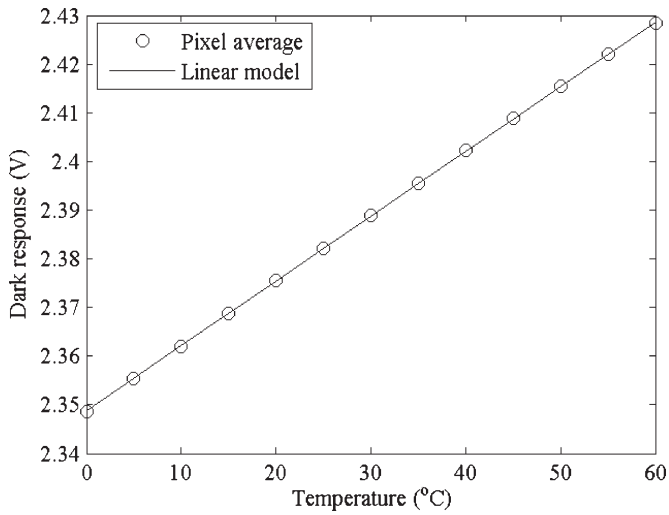

Fig. 2. Average dark response of 100 simulated pixels versus temperature. Regression analysis shows the relationship to be very linear, i.e., $R^2 = 100\%$.

pixels [21], which were built in a 0.35-μm 3.3-V process by the Institute for Microelectronics Stuttgart.

A simultaneous parametric, dc, and Monte Carlo analysis was performed. The parametric analysis varied the temperature from 0- to 60-°C in 5-°C steps for a total of 13 set points. The dc analysis varied the photocurrent in half-decade steps from 1 pA to 1 μA for a total also of 13 set points. Third, the Monte Carlo analysis repeated the simulation 100 times, each time with different parameters for each transistor according to statistical distributions that are specified by AMS to simulate device mismatch. This approach simulates the response over temperature and photocurrent of 100 randomly selected pixels from a larger image sensor that suffers from FPN.

The simulated light response is denoted by y_{hij}, where h indexes the temperature T_h (with $1 \leq h \leq 13$), i indexes the photocurrent x_i (with $1 \leq i \leq 13$), and j indexes the pixel (with $1 \leq j \leq 100$). In the literature on logarithmic cameras, noise levels may be quoted as a percentage of the change in the response due to a one-decade change in the stimulus. Thus, it is worth noting that the light response changed, on average, over all temperatures and pixels by 40 mV per decade of the photocurrent change. By setting the photocurrent to zero and carrying out the parametric and Monte Carlo analysis as before with the same random seed, the dark response of the pixels, which is denoted by y_{h0j}, was simulated over the same temperatures and device parameters as before.

The light response at 30 °C was used to calibrate the double-variation model in the literature [12], which does not consider temperature dependence. The calibrated model was then used to account for the FPN at other temperatures. Fig. 1 shows the residual error per image versus temperature and photocurrent for the calibration at 30 °C and the extrapolation to other temperatures. A cross section of this surface at any photocurrent is v-shaped, with a minimum at 30 °C, and a cross section at any temperature is horizontal and not w-shaped, as reported in the literature. The w-shape arose when the double-variation model was used to calibrate a camera that actually obeyed the triple-variation model, i.e., where the photodiode leakage current varied from pixel to pixel. Since AMS did not supply statistical distributions for the parameters of the diode model, the leakage current did not vary in the Monte Carlo simulation.

Consequently, at any one temperature, double variation is an excellent model of FPN in the simulated pixels, but it is inaccurate away from the temperature of calibration. The degradation is graceful, which means that the temperature dependence of FPN may be ignored if the temperature range is sufficiently small, and the temperature of calibration falls in the middle. At 30 °C alone, the residual error over all photocurrents and pixels was 0.29 mV or 0.73% of a decade. Over the 0- to 60-°C range, the residual error was 0.49 mV or 1.2% of a decade.

Fig. 2 shows that the average dark response $\bar{y}_{h0}$ of the simulated pixels may be accurately described as a linear proxy of temperature T_h over the 0- to 60-°C range. With this assumption confirmed, the light response was used to evaluate the temperature proxy method. Fig. 3 shows the residual error per image, which is defined in (41), versus temperature and photocurrent. The error is independent of both variables, unlike in Fig. 1, which means that the temperature proxy model is suitable for extrapolation over wide ranges. Moreover, the overall residual error, which is defined in (39), is equal to 0.29 mV or 0.73% of a decade. This result is as good as the double-variation result at 30 °C alone and is better than the double-variation result over the 0- to 60-°C range.

Apart from the absence of bias variation, the simulation is mainly limited in three ways when compared with an experiment. First, the schematic may not contain all the circuit elements of a real imager, such as parasitic resistors, capacitors, diodes, and transistors. Second, the models that are used by the simulator to describe the behavior of circuit elements are only the approximations of the behavior of real elements. However, these BSIM3 models are far more sophisticated than the Levels 1–3 models that are used by the theory of Sections II and III. Third, quantization and temporal noise have not been simulated. Hence, over a range of conditions, the residual error per image in Fig. 3 measures the deviation between the temperature proxy model of (30), which is derived from (1) and

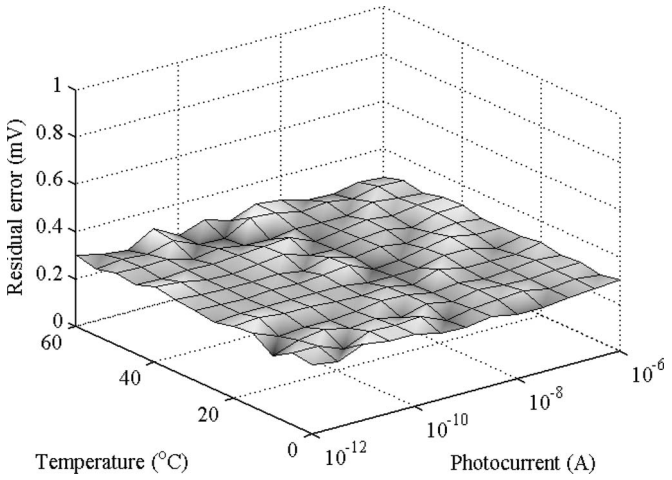

Fig. 3. Residual error per image versus temperature and photocurrent for the calibration of the temperature proxy model to simulated data. The overall residual error is 0.29 mV or 0.73% of a decade.

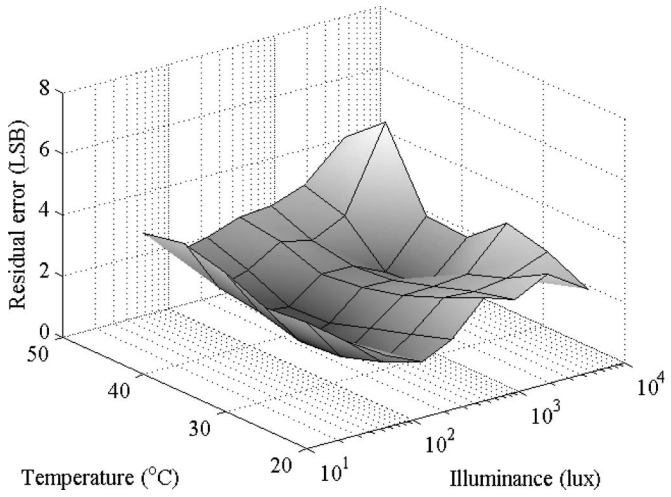

Fig. 4. Residual error per image versus temperature and illuminance for the calibration of the established double-variation model [12] to Fuga 15RGB data at 35 °C with subsequent extrapolation to other temperatures. The overall residual error is 2.4 LSB or 5.7% of a decade.

(11)–(13), and the complex model of the simulator. One can conclude by the uniform fraction-of-a-millivolt result that the model is excellent in the absence of bias variation.

V. Experiment

An experiment was performed using a Fuga 15RGB camera from C-Cam Technologies [22]. Although it is a color camera, the Fuga 15RGB is treated here as a monochromatic one. Since the red, green, and blue color filters, which overlay the pixels in sequence, are designed to reproduce the spectral response of the human eye, the stimulation of the underlying photodiodes was approximately constant for the white light used in the experiment.

The Fuga 15RGB has an on-chip 8-bit ADC [23]. Due to FPN, which causes a wide variation in pixel response even for a uniform scene, and since the experiment drove the camera over a wide dynamic range, the response may saturate the ADC range. However, the camera allows the ADC range to be shifted by a programmable offset. By changing the ADC offset, saturated pixels may be brought within the ADC range, adding two extra bits of information per pixel [11].

For the experiment, the Fuga 15RGB was placed in an oven, together with a 2850-lm compact fluorescent lamp. Images of a uniformly illuminated sheet of white paper, which was also in the oven, were taken. The temperature could only be varied from a low of 20 °C, since an oven cannot cool below room temperature, to a high of 50 °C, since the plastic camera housing melted above this temperature. As the oven's own heating element produced heat too quickly, so that the temperature inside the camera could not keep pace, and as the thermostatic control was unstable at low temperatures, it was not used. Instead, the insulated interior of the oven was left to warm slowly, at an average rate of 3 °C per hour, using 44.5 W of power dissipated by the lamp.

The illuminance of the white paper was measured with a light meter to be 4500 lx, which did not vary with temperature. Images of this sheet were taken for every 5-°C change in the temperature, which was measured using the oven's digital thermometer, for a total of seven set points. At each temperature, images were taken with the aperture setting varied from 1.8 to 16 f-stops to generate seven illuminance set points. An image was also taken with the aperture closed.

The fluorescent lamp was used to provide ample light but little heat—a tungsten lamp of equal brightness would make the oven temperature rise too quickly. Unfortunately, the intensity of the light cast by the fluorescent lamp oscillated at a high frequency, which was recorded by the camera, although invisible to the eye. The oscillation manifested itself as narrow horizontal bands that vertically moved across consecutive image frames. This beating effect, which was a source of error, was reduced by averaging multiple frames to compose each image since the bands fell in different positions in different frames.

As has recently been explained in the literature [14], the transient response of the read-out circuit contributes to the FPN in the Fuga 15RGB. Whereas Sections II–IV did not consider such dependence, it is impossible to avoid it in an experiment. Although transient-dependent FPN may be calibrated to some degree using the steady-state methods derived here, a better solution is to improve the design of the read-out circuit. Fortunately, the phenomenon may substantially be reduced by discarding the first 100 columns of each image.

Thus, although the Fuga 15RGB has a 512×512 array of pixels, only the pixels in the last 412 columns are counted here. The light response of the jth pixel (where $1 \leq j \leq 512 \times 412$) at temperature T_h (where $1 \leq h \leq 7$) and illuminance x_i (where $1 \leq i \leq 7$) is denoted by y_{hij}. Similarly, the dark response of the jth pixel at temperature T_h is denoted by y_{h0j}. The light response changed, on average, over all temperatures and pixels, by 43 least significant bits (LSBs) per decade of illuminance change.

To compare this work to previous work, the light response at 35 °C was used to calibrate the established double-variation model [12], which does not consider temperature dependence. The calibrated model was then used to account for the FPN over the entire temperature and illuminance range of the experiment. Fig. 4 shows the residual error per image versus temperature

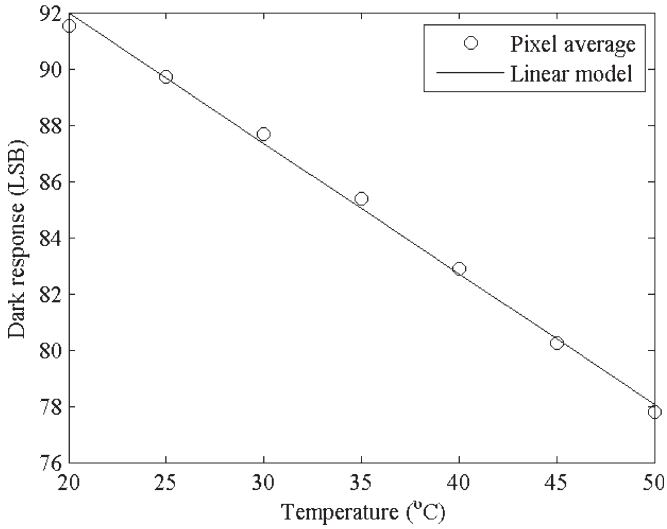

Fig. 5. Average dark response of Fuga 15RGB pixels versus temperature. Regression analysis shows the relationship to be very linear, i.e., $R^2 = 99.6\%$.

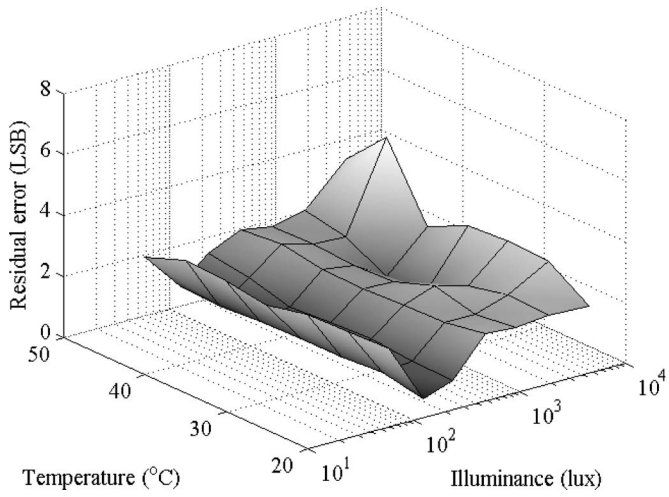

Fig. 6. Residual error per image versus temperature and illuminance for the calibration of the temperature proxy model to Fuga 15RGB data. The overall residual error is 2.0 LSB or 4.8% of a decade.

and illuminance for the calibration at 35 °C and the extrapolation to other temperatures. A cross section of this surface at any illuminance has a minimum at 35 °C, as one might expect. A cross section at any temperature is similar to the w-shape described in the literature.

The w-shape arose when the double-variation model was used to calibrate a camera that obeyed the triple-variation model, i.e., where the photodiode leakage current varied from pixel to pixel, as in the Fuga 15RGB. Although a method exists to calibrate the triple-variation model at any one temperature [12], giving a flat shape to the residual error per image, it requires nonlinear optimization and so has not been adapted yet for use across multiple temperatures.

Thus, at any one temperature, double variation is the best model of FPN that avoids nonlinear optimization, but it is inaccurate away from the temperature of calibration. The degradation is graceful, which means that the temperature dependence of FPN may be ignored if the temperature range is sufficiently small, and the temperature of calibration falls in the middle. At 35 °C alone, the residual error, over all illuminances and pixels, was 2.0 LSB or 4.8% of a decade. For the 20- to 50-°C range, the residual error was 2.4 LSB or 5.7% of a decade.

The first task in evaluating the temperature proxy method of Section III is to check its principal assumption. Fig. 5 plots the average dark response $\bar{y}_{h0}$ of the Fuga 15RGB pixels versus temperature T_h. Because the simulation and the experiment involve different technologies (i.e., a 0.35-μm 3.3-V AMS one and a 0.7-μm 5-V Alcatel one [24]), design choices (e.g., device sizes), and other factors (e.g., ADC effects), values in Figs. 2 and 5 are not comparable. However, one may explain why the lines slope in opposite directions. Higher photocurrents lead to lower voltages in the simulation due to an inverting load in the pixel, whereas higher illuminances lead to higher integers in the experiment due to a negative ADC gain in the Fuga 15RGB. The simulation did not include an ADC with a negative gain, and therefore, the slopes in Figs. 2 and 5 have opposite signs.

Over a 20- to 50-°C range, the average dark response ranges from 92 to 78 LSB and may be described as a linear proxy of the temperature with a 0.34-LSB standard deviation. With this assumption confirmed, the light response of the Fuga 15RGB pixels was used to evaluate the temperature proxy method. After calibration, the overall residual error, which is defined in (39), is equal to 2.0 LSB or 4.8% of a decade. This result, which is obtained over a range of temperatures, is as good as the double-variation result at 35 °C alone and is better than the double-variation result over the 20- to 50-°C range.

Fig. 6 shows the residual error per image, which is defined in (41), versus temperature and illuminance. Although the error depends on illuminance, approximately having a w-shape for any given temperature, it is independent of temperature except at high illuminance, when the beating effects of the fluorescent lamp and the transient response of the Fuga 15RGB become significant. Thus, the temperature proxy model accounts for the temperature-dependent FPN in Fuga 15RGB images, but is limited by bias variation in accounting for illumination-dependent FPN.

The experiment mainly differs in three ways when compared with the simulation. First, for lack of suitable equipment, it was difficult to use a wide temperature range with the Fuga 15RGB. Second, the transient response of the read-out circuit and the oscillation of the light source significantly affected the experimental results. Third, since the experiment included bias variation, as well as quantization and temporal noise, the results are necessarily worse than those of the simulation. Nonetheless, considering the work in the literature on w-shaped graphs of residual error versus illuminance [12], the experimental results support the theoretical results of Sections II and III and generally agree with the simulation results of Section IV.

VI. Conclusion

The response of a logarithmic pixel depends on temperature, as well as illuminance, because the threshold voltages, the current gains, the subthreshold slope, the crossover current, and the leakage current of the circuit depend on temperature. Using semiconductor physics to extend the prior work by Joseph

and Collins [12], a model of pixel response to temperature and illuminance has been derived, which incorporates proto-offset, protogain, and protobias parameters. A variation of these parameters from pixel to pixel causes FPN, which depends on temperature.

Based on the above model, a simpler *temperature proxy* model has been proposed, as well as a method that is based on maximum-likelihood estimation to calibrate and correct the FPN. Calibration requires the light and dark responses of pixels to a uniform stimulus at several temperatures and illuminances. However, it does not require the measurement of any temperature or illuminance. When the average dark response of all pixels is a linear function of temperature, the light response of any pixel is a linear function of the average dark and light responses of all pixels, given the same temperature and illuminance. Correction of FPN in an arbitrary image follows readily. For calibration and correction, bias variation has been neglected to avoid nonlinear optimization.

Simulation and experiment have been used in a complementary fashion to validate the theory. They have shown that FPN may be calibrated to give a residual error per image that is independent of temperature, unlike with the established double-variation method [12], which employed a model that did not factor out temperature. Since bias variation has been neglected, the residual error per image does depend on illuminance, as predicted in the literature. Furthermore, the degradation of the double-variation model is graceful, which means that the temperature dependence of FPN may be safely ignored for a deviation up to $\pm 10\ ^{\circ}\mathrm{C}$ with respect to the temperature of calibration.

To effectively deal with FPN over a wide range of temperature and illuminance, the method presented here provides a good starting point, i.e., one that is based on semiconductor physics, is statistically sound, and avoids unnecessary measurement. Further work is needed to incorporate bias variation while retaining the advantages of the proposed method.

REFERENCES

[1] A. El Gamal and H. Eltoukhy, "CMOS image sensors," *IEEE Circuits Syst. Mag.*, vol. 21, no. 3, pp. 6–20, May 2005.

[2] O. Yadid-Pecht, "Wide-dynamic-range sensors," *Opt. Eng.*, vol. 38, no. 10, pp. 1650–1660, Oct. 1999.

[3] "Vision for machines," *One Megapixel CMOS Stop Action Camera Family*, Feb. 2004, DALSA. Tech. Rep.

[4] V. Schneider, "Fixed-pattern correction of HDR image sensors," in *Proc. Ph.D. Res. Microelectron. Electron. Conf.*, Jul. 2005, pp. 99–102.

[5] G. Storm, R. Henderson, J. E. D. Hurwitz, D. Renshaw, K. Findlater, and M. Purcell, "Extended dynamic range from a combined linear-logarithmic CMOS image sensor," *IEEE J. Solid-State Circuits*, vol. 41, no. 9, pp. 2095–2106, Sep. 2006.

[6] *High-Dynamic-Range (HDR) Vision*, Series in Advanced Microelectronics, vol. 26, B. Hoefflinger, Ed. New York: Springer-Verlag, 2007.

[7] S. Kavadias, B. Dierickx, D. Scheffer, A. Alaerts, D. Uwaerts, and J. Bogaerts, "A logarithmic response CMOS image sensor with on-chip calibration," *IEEE J. Solid-State Circuits*, vol. 35, no. 8, pp. 1146–1152, Aug. 2000.

[8] M. Loose, K. Meier, and J. Schemmel, "A self-calibrating single-chip CMOS camera with logarithmic response," *IEEE J. Solid-State Circuits*, vol. 36, no. 4, pp. 586–596, Apr. 2001.

[9] L.-W. Lai, C.-H. Lai, and Y.-C. King, "A novel logarithmic response CMOS image sensor with high output voltage swing and in-pixel fixed-pattern noise reduction," *IEEE Sensors J.*, vol. 4, no. 1, pp. 122–126, Feb. 2004.

[10] D. Joseph and S. Collins, "Temperature dependence of fixed pattern noise in logarithmic CMOS image sensors," in *Proc. IEEE Instrum. Meas. Technol. Conf.*, May 2007, pp. 1–6.

[11] D. Joseph, "Modelling and calibration of logarithmic CMOS image sensors," Ph.D. dissertation, Univ. Oxford, Oxford, U.K., Sep. 2002.

[12] D. Joseph and S. Collins, "Modeling, calibration, and correction of nonlinear illumination-dependent fixed pattern noise in logarithmic CMOS image sensors," *IEEE Trans. Instrum. Meas.*, vol. 51, no. 5, pp. 996–1001, Oct. 2002.

[13] D. Joseph and S. Collins, "Modeling, calibration, and rendition of color logarithmic CMOS image sensors," *IEEE Trans. Instrum. Meas.*, vol. 52, no. 5, pp. 1581–1587, Oct. 2003.

[14] D. Joseph and S. Collins, "Transient response and fixed pattern noise in logarithmic CMOS image sensors," *IEEE Sensors J.*, vol. 7, no. 8, pp. 1191–1199, Aug. 2007.

[15] B. Choubey, S. Aoyama, S. Otim, D. Joseph, and S. Collins, "An electronic-calibration scheme for logarithmic CMOS pixels," *IEEE Sensors J.*, vol. 6, no. 4, pp. 950–956, Aug. 2006.

[16] S. Otim, B. Choubey, D. Joseph, and S. Collins, "Characterisation and simple fixed pattern noise correction in wide dynamic range 'logarithmic' imagers," *IEEE Trans. Instrum. Meas.*, vol. 56, no. 5, pp. 1910–1916, Oct. 2007.

[17] G. F. Marshall and S. Collins, "A high dynamic range front end for automatic image processing applications," in *Proc. SPIE—Advanced Focal Plane Arrays* and *Electronic Cameras II*, May 1998, vol. 3410, pp. 176–185.

[18] D. P. Foty, *MOSFET Modeling With SPICE: Principles and Practice*. Upper Saddle River, NJ: Prentice–Hall, 1997.

[19] *0.35 μm CMOS Process Parameters*, Austria Microsystems, Unterpremstätten, Austria. Document 9933016.

[20] *0.35 μm CMOS Design Rules*, Austria Microsystems, Unterpremstätten, Austria. Document 9931032.

[21] *HDRC VGA Imager and Camera Data and Features*, IMS Chips, Inst. Microelectron. Stuttgart, Stuttgart, Germany, Sep. 2000. Tech. Rep.

[22] *Fuga Data Sheets*, C-Cam Technologies, Vector Int., Leuven, Belgium, Apr. 1998. Tech. Rep.

[23] *Introduction Software for Fuga RGB*, C-Cam Technologies, Vector Int., Leuven, Belgium, Apr. 1998.

[24] B. Dierickx, *RE: Fuga 15d Query*, Jul. 2002. Electronic mail.

Dileepan Joseph (M'96) received the B.Sc. degree in computer engineering from the University of Manitoba, Winnipeg, MB, Canada, in 1997 and the D.Phil. degree in engineering science from the University of Oxford, Oxford, U.K., in 2003. His doctoral research concerned logarithmic complementary metal–oxide semiconductor image sensors.

Since 2004, he has been with the Faculty of Engineering, University of Alberta, Edmonton, AB, Canada, where he has continued working on imaging science.

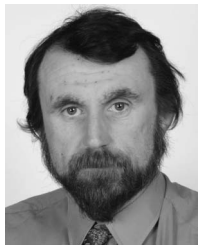

Steve Collins (M'03) received the B.Sc. degree in theoretical physics from the University of York, York, U.K., in 1982 and the Ph.D. degree from the University of Warwick, Coventry, U.K., in 1986.

From 1985 to 1997, he was with the Defence Research Agency, Malvern, U.K., working on various topics, including the origins of $1/f$ noise in metal–oxide–semiconductor field-effect transistors and analog information processing. Since 1997, he has been with the University of Oxford, Oxford, U.K., where he has continued his interest in smart imaging sensors and nonvolatile analog memories.